The Effect of Twinning and Slip on the Bauschinger Effect of Hadfield Steel Single Crystals

IBRAHIM KARAMAN, HUSEYIN SEHITOGLU, Y.I. CHUMLYAKOV, HANS J. MAIER, and I.V. KIREEVA

The Bauschinger effect (BE) in single crystals of Hadfield manganese steel (Fe, 12.3Mn, 1.0C in wt pct) was studied for three crystallographic orientations, [$\bar{1}$11], [$\bar{1}$23], and [001]. Both forward tension-reverse compression (FT/RC) and forward compression-reverse tension (FC/RT) loading schemes were used to investigate the role of deformation history on the BE. The evolution of stress-strain response and a dimensionless Bauschinger parameter were used to study the BE. The BE stems from long-range back stress generated by the dislocation pileups at the twin and localized slip boundaries. Twinning boundaries present a strong obstacle and lead to a strong BE. If localized slip followed twinning, permanent softening was evident, such as in the case of the [$\bar{1}$11] FT/RC scheme. Localized slip and multiple slip in the forward loading provided a transient effect in the stress-strain response without a significant permanent softening. Hadfield steel single crystals have demonstrated a high BE for orientations conducive to combined twinning/slip deformation. The BE increased with increasing prestrain, then saturated and started to decrease, in contrast with precipitation-hardened alloys. A unique strain-hardening approach along with the back stress calculation was introduced into a viscoplastic self-consistent (VPSC) formulation. The strain-hardening formulation incorporates length scales associated with spacing between twin lamellae. The simulations correctly predicted the BE and the stress-strain response for both forward and reverse loading.

I. INTRODUCTION

THE interest in the work-hardening mechanisms of metals deforming by twinning and slip has been continuously increasing in recent years. To establish relationships for describing the complex response of metals in service conditions, Bauschinger experiments have proved valuable. Johann Bauschinger[1] was the first who examined steels through a series of successive tension and compression loading applications and demonstrated the lowering of the yield point during reverse deformation.

To date, almost all Bauschinger studies have focused on dispersion-hardened alloys that exhibit a large Bauschinger effect (BE).[2–6] There are also other studies on pure metals, such as Cu and Al,[3,7] on steels,[8] and on low stacking fault energy (SFE) metals, such as Cu-Al.[9] According to the aforementioned studies, the observed BE is caused by the development of internal stress during forward loading. This stress serves as a back stress that resists the dislocation motion in forward straining while assisting the deformation during the reverse straining.

Although back stresses mostly originate from Orowan shear loops around dispersoids, it has been shown that dislocation tangles can act as hard but deformable barriers in a relatively soft matrix.[7] Moreover, the characteristics of the dislocations can be another major factor in the BE, according to Abel and Muir.[9]

The studies on the BE and the relative roles of work-hardening mechanisms have been mostly focused on materials that deform only by slip. To our knowledge, no detailed Bauschinger studies have been reported that elucidate the relative importance of twinning and slip and their interaction. Therefore, the current work will clarify the role of twinning on the BE of Hadfield manganese steels.

Hadfield steel is a stable austenitic steel with nominal manganese and carbon compositions of 12 to 14 pct and 1.0 to 1.3 pct, respectively. It is characterized by a high strain-hardening (upward stress strain) curve and by the absence of a recovery regime typical of Al and Cu alloys. Recently, the authors[10] demonstrated orientation dependence and tension-compression asymmetry in deformation mechanisms and strain-hardening behavior under uniaxial loading. It was shown that the primary reason for the upward curvature in stress-strain response was the strong interaction of slip and twinning in orientations preferably oriented for twinning. Therefore, it is of great interest to explore both the interaction of these mechanisms and the effect of these mechanisms on the stress-strain response.

A number of parameters have been proposed to characterize the BE in metals. Some of the parameters proposed include β_σ (lowering of the yield stress), β_ε (the relative Bauschinger strain), β_E (the relative energy saving in reverse deformation), and permanent softening.[6,11] Although these parameters are unambiguously defined in polycrystals, the added complication in the single crystals of the present material is that the deformation mechanism is orientation dependent.[10,12] Moreover, if β_ε and β_E were used for single crystals, the comparison of the BE would be misleading because some orientations exhibit Lüder's type deformation,

IBRAHIM KARAMAN, formerly Research Associate, Department of Mechanical and Industrial Engineering, University of Illinois, is Assistant Professor, Department of Mechanical Engineering, Texas A & M University, College Station, TX 77843. HUSEYIN SEHITOGLU, Grayce Wicall Gauthier Professor, is with the Department of Mechanical and Industrial Engineering, University of Illinois, Urbana, IL 61801. Y.I. CHUMLYAKOV, Professor, and I.V. KIREEVA, Research Scientist, is with the Siberian Physical-Technical Institute, Tomsk 634050, Russia. HANS J. MAIER, Professor, is with the University of Paderborn, Lehrstuhl f. Werkstoffkunde, (Materials Science), D-33095 Paderborn, Germany.

Manuscript submitted February 21, 2000.

while others develop linear hardening. These differences in initial strain hardening may affect the interpretation of these parameters. In this study, for the comparison of the BE, Moan and Embury's[3] nondimensional back stress approach will be utilized.

Phenomenological continuum plasticity approaches[2,13] and other physically sound microstructural theories[3,7,14] have been proposed to predict the BE. Moan and Embury[3] predicted the long-range back stresses (decrease in yield stress) in single crystals of particle-hardened Al-4 pct Cu. Pedersen *et al.*[7] demonstrated in work-hardened pure copper that dislocation tangles act as hard but deformable inclusions in a soft matrix, leading to a significant barrier for forward dislocation motion and, thus, a significant BE.

In the present study, a unique approach will be proposed that considers twin boundaries as hard but penetrable obstacles and that utilizes the viscoplastic self-consistent (VPSC) plasticity model.[12] The dislocation pileup due to twin boundaries generates a long-range internal stress field, which leads to a significant BE. The magnitude of the back stress will be predicted by the modified Moan and Embury model, which considers the orientation and stress-state dependence of Hadfield steel single crystals. The proposed model simulates both forward and reverse stress-strain response, and considers both twinning and slip as deformation mechanisms.

This article presents unique results in single crystal deformation with alternate compressive and tensile prestrains, along with microstructural observations. The VPSC model predicts the stress-strain response and the BE for different orientations and for different stress states.

The outline of the article is as follows. In Section II, the experimental details will be provided. In Section III, the results of the Bauschinger experiments will be presented, along with representative microstructural observations. In Section IV, the constitutive equations for single crystals and the essentials of the VPSC approach will be briefly described. Section V will include a detailed explanation of the prediction of back stress and of our hardening approach. Finally, in Section VI, simulations and experiments will be compared, along with a discussion of the results.

II. EXPERIMENTAL TECHNIQUES

The material used in this study was a Hadfield steel with a composition of 12.3 wt pct Mn, 1.03 wt pct C, and balance Fe. Single crystals were grown with the Bridgman technique in a He atmosphere. Electrodischarge machining was used to cut the regular dog-bone-shaped flat Bauschinger specimens with nominal dimensions of $8 \times 3 \times 2.5$ mm in the gage section. Specimens were then solution treated and water quenched from 1373 K after 1 hour. Tests were performed at room temperature with a hydraulic Instron test machine. The strain rate of $5 \times 10^{-5}\ s^{-1}$ was used and the specimens were inspected to ensure buckling did not occur. Experiments were repeated on two to three companion specimens to check repeatability. For transmission electron microscopy (TEM) analysis, the samples were prepared by mechanical grinding and twin jet electropolishing. The electropolishing agent is a mixture of 80 g of anhydrous sodium chromate and 400 mL of glacial acetic acid. Thin foils were examined in a PHILIPS* CM 200 electron microscope operated at 200 kV.

*PHILIPS is a trademark of Philips Electronic Instruments Corp., Mahwah, NJ.

III. EXPERIMENTAL RESULTS

A. *Deformation Mechanisms*

In the present study, three different orientations, $[\bar{1}11]$, $[\bar{1}23]$, and [001], were chosen to exemplify the standard stereographic triangle. These orientations were chosen to compare single *vs* multislip and twinning *vs* slip deformation mechanisms on the BE. Prestraining was applied successively in tension and compression to evaluate the role of the stress state on the BE.

Table I lists the Schmid factors for slip and twinning both under tension and compression as well as the observed macroscopic deformation mechanisms. These mechanisms are established upon microscopical observations in the present work and also in the preceding studies.[10,12,15,16] We note that the orientations $[\bar{1}11]$ and $[\bar{1}23]$ demonstrate similar deformation mechanisms but different strain-hardening behavior, due to the number of systems activated.

The representative stress-strain responses for each orientation are illustrated for two different cases (tensile and compressive prestraining) in Figures 1 through 6. Figure 1 shows that the tensile deformation of a specimen with $[\bar{1}11]$ orientation results in twinning followed by localized slip under compression. The notable surface relief was determined to be twinning through a repolishing and etching scheme[10] and through X-ray diffraction.[12] The localized slip observations on the surface of the samples are found to be macro-shear-band (MSB) formations due to the misorientation of 9 deg, as determined by Electron Back Scattering Pattern (EBSP) measurements (Figure 7). The prevailing deformation mechanisms were confirmed by a detailed TEM study.[10] Similar methods were used to construct Table I for other cases.

B. *Bauschinger Experiments in $[\bar{1}11]$, $[\bar{1}23]$, and [001] Orientations*

Figures 1 through 3 are grouped to show the stress states and orientations in which twinning is the primary deformation mechanism during prestraining. The cases in Figures 4 and 5 experience MSBs in the prestraining cycle. Figure 6 is the only case in which localized slip or twinning is not observed in the first cycle.

The deformation along the $[\bar{1}11]$ orientation under tensile preloading (Figure 1) occurs *via* twinning and results in slip and MSB formation under successive compressive loading. In compressive loading, a transient nonlinear region with a lower microyield point compared to the tensile forward loading is visible, and then a significant permanent softening (as defined in Figure 1) develops. If the stresses are scaled based on the appropriate Schmid factors from Table I, the magnitude of this permanent softening would be more pronounced. This lowering in the microscopic yielding and the permanent softening indicates a significant BE.

A typical surface relief pattern for the $[\bar{1}11]$ orientation

Table I. Calculated Schmid's Factors and Observed Macroscopic Deformation Mechanisms for Two Different Loading Schemes (FT/RC Represents the Bauschinger Experiment with Tensile Preload, and FC/RT Is the One with Compressive Preload)

	Schmid's Factors				Observed Macroscopic Deformation Mechanisms			
	Tension		Compression		FT/RC		FC/RT	
Orientation	Twinning	Slip	Twinning	Slip	Tension	Compression	Compression	Tension
[$\bar{1}$11]	0.314 (3 sys.)	0.272 (6 sys.)	0.157 (6 sys.)	0.272 (3 sys.)	twinning	slip (MSB)	slip (MSB)	twinning
[$\bar{1}$23]	0.471 (1 sys.)	0.466 (1 sys.)	0.336 (1 sys.)	0.466 (1 sys.)	twinning	slip (MSB)	slip (MSB)	twinning
[001]	0.236 (8 sys.)	0.408 (8 sys.)	0.471 (4 sys.)	0.408 (8 sys.)	slip	twinning	twinning	slip

The term "MSB" represents macro shear band and "sys." represents system.

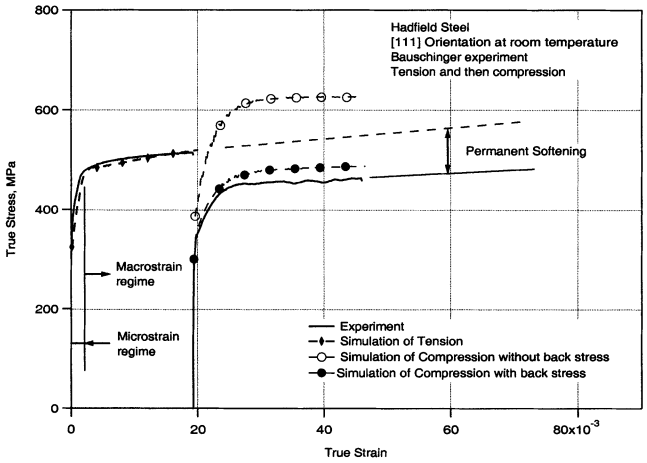

Fig. 1—True stress–true strain behavior of the [$\bar{1}$11] orientation under FT/RC loading. Both experimental results and the simulations are shown. Note the definition of permanent softening and the differentiating between micro- and macrostrain regimes.

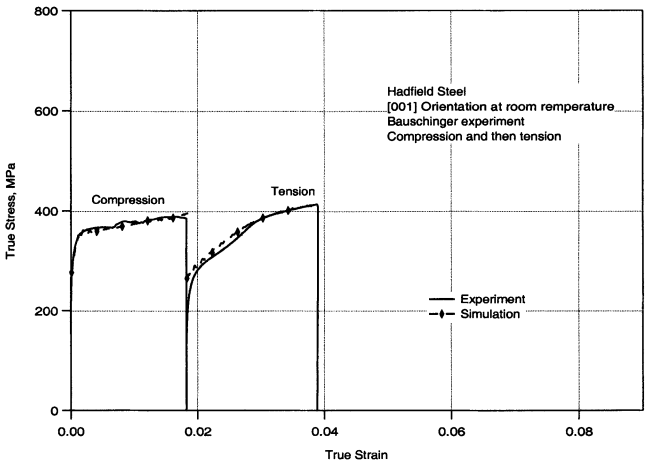

Fig. 2—True stress–true strain behavior of the [001] orientation under FC/RT loading. Both experimental results and the simulations are shown.

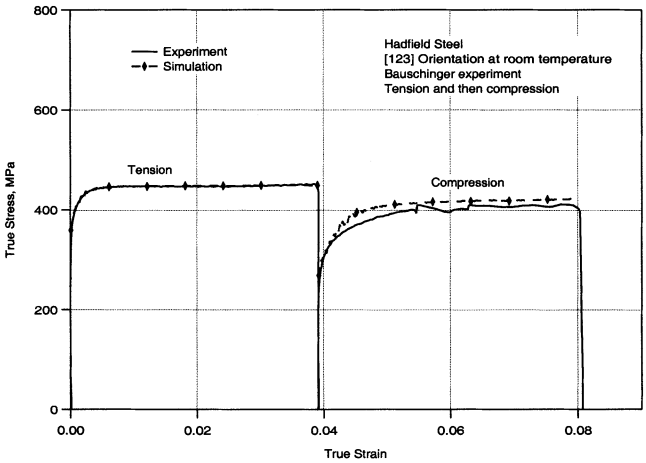

Fig. 3—True stress–true strain behavior of the [$\bar{1}$23] orientation under FT/RC loading. Both experimental results and the simulations are shown.

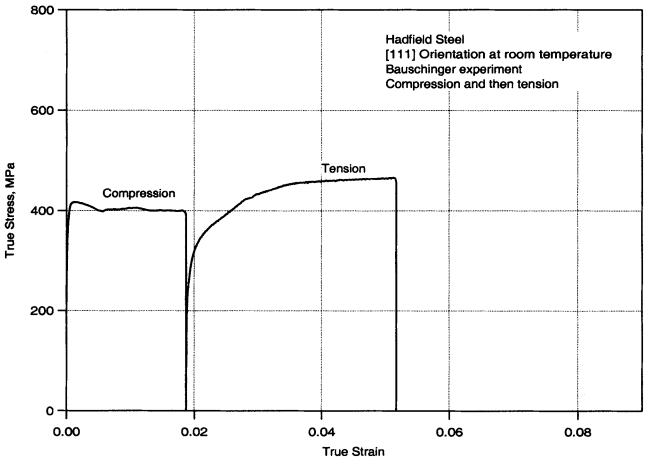

Fig. 4—True stress–true strain behavior of the [$\bar{1}$11] orientation under FC/RT loading.

after forward tensile and reverse compressive (FT/RC) loading is presented in Figures 8(a) and (b). For the forward compressive and reverse tensile (FC/RT) loading, Figures 8(c) and (d) show the surface relief formations.

In the case of [001] orientation under compressive forward loading (Figure 2), which leads to twinning, a large drop in yield level is evident together with an extended nonlinear transient region. The permanent softening exists and it is more pronounced when resolved stress components are considered. On the other hand, the present orientation under the tensile forward and compressive reverse loading (Figure 6)

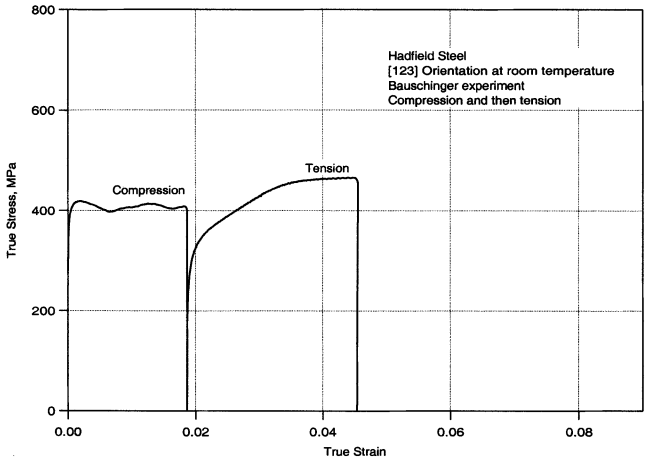

Fig. 5—True stress–true strain behavior of the [$\bar{1}$23] orientation under FC/RT loading.

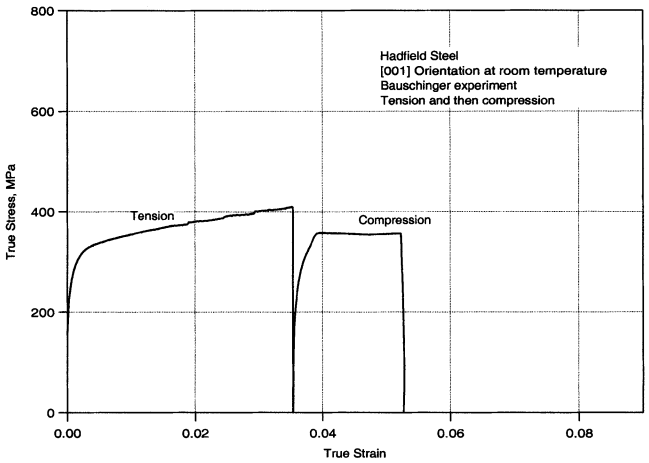

Fig. 6—True stress–true strain behavior of the [001] orientation under FT/RC loading.

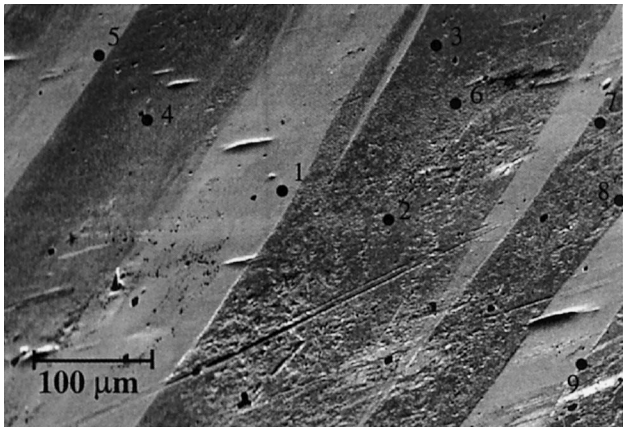

(*a*)

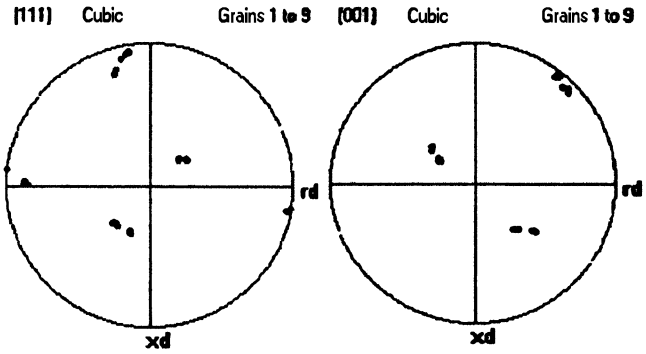

(*b*)

Fig. 7—(*a*) SEM image of the [$\bar{1}$11] compression sample deformed to 3 pct strain. (*b*) [111] and [001] pole figures obtained by EBSP for the different regions marked 1 through 9 in (a). From the EBSP data, the misorientation between the bright and the dark regions is calculated to be about 9 deg. The surface of the sample is normal to [211].

exhibits a narrow transient region in between microscopic and macroscopic yielding, and permanent softening is not as pronounced as in the compressive forward and tensile reverse loading (Figure 2).

The [$\bar{1}$23] orientation produces results similar to the [$\bar{1}$11] orientation; however, the permanent softening is not as pronounced as in the latter case. Figures 8(a) through (d) represent the macroscopic deformation mechanisms for the [$\bar{1}$23] orientation as well. The main difference in the microscopic observations between the [$\bar{1}$11] and [$\bar{1}$23] orientations is that, in the [$\bar{1}$23] case, localized deformations (twinning or MSB) are distributed more diffusely than in the [$\bar{1}$11] case.

In the [001] orientation, multiple slip is evident with no clear localization under tension. Double twinning is the primary deformation mechanism under compression in both loading sequences (Figures 8(e) and (f)).

The results presented in Figures 1 through 8 indicate that, whenever twinning is the primary deformation mechanism in forward loading, there is a significant lowering in the reverse yield strength accompanied by permanent softening. This produces a large BE. In the case of localized slip (MSB formation) at low strain levels, in the compressive forward loading of the [$\bar{1}$11] and [$\bar{1}$23] orientations, MSBs assist the reverse deformation under tension; however, this is a transient effect without significant permanent softening. If slip localization is not the mode of early deformation, as in the case of the [001] orientation, no significant BE is observed as compared to the previous cases.

C. *Determination of Bauschinger Parameter Based on Remote Stresses*

The comparison of the magnitude of the BE is quite intricate, especially for single crystals. In this study, a nondimensional stress parameter is defined to compare the magnitudes of the BE following the treatment of Moan and Embury[3] and Pedersen *et al.*[7] The flow stress σ_f at a certain forward strain can be defined as

$$\sigma_f = \sigma_0 + \sigma_d + \sigma_b \qquad [1]$$

where σ_0 is the initial yield of the material, which is mainly lattice friction together with solid solution hardening; σ_d is a term due to forest dislocation hardening; and σ_b is the long-range back stress. The sources of this back stress can be unrelaxed Orowan loops around particles,[3] dislocation pileups because of dislocation tangles,[7] twinning, and MSBs. The σ_0 and σ_d are nondirectional because they oppose flow in both forward and reverse loading. However, σ_b aids deformation in reverse loading. The onset of plastic deformation takes place at a stress σ_{rev}, which is

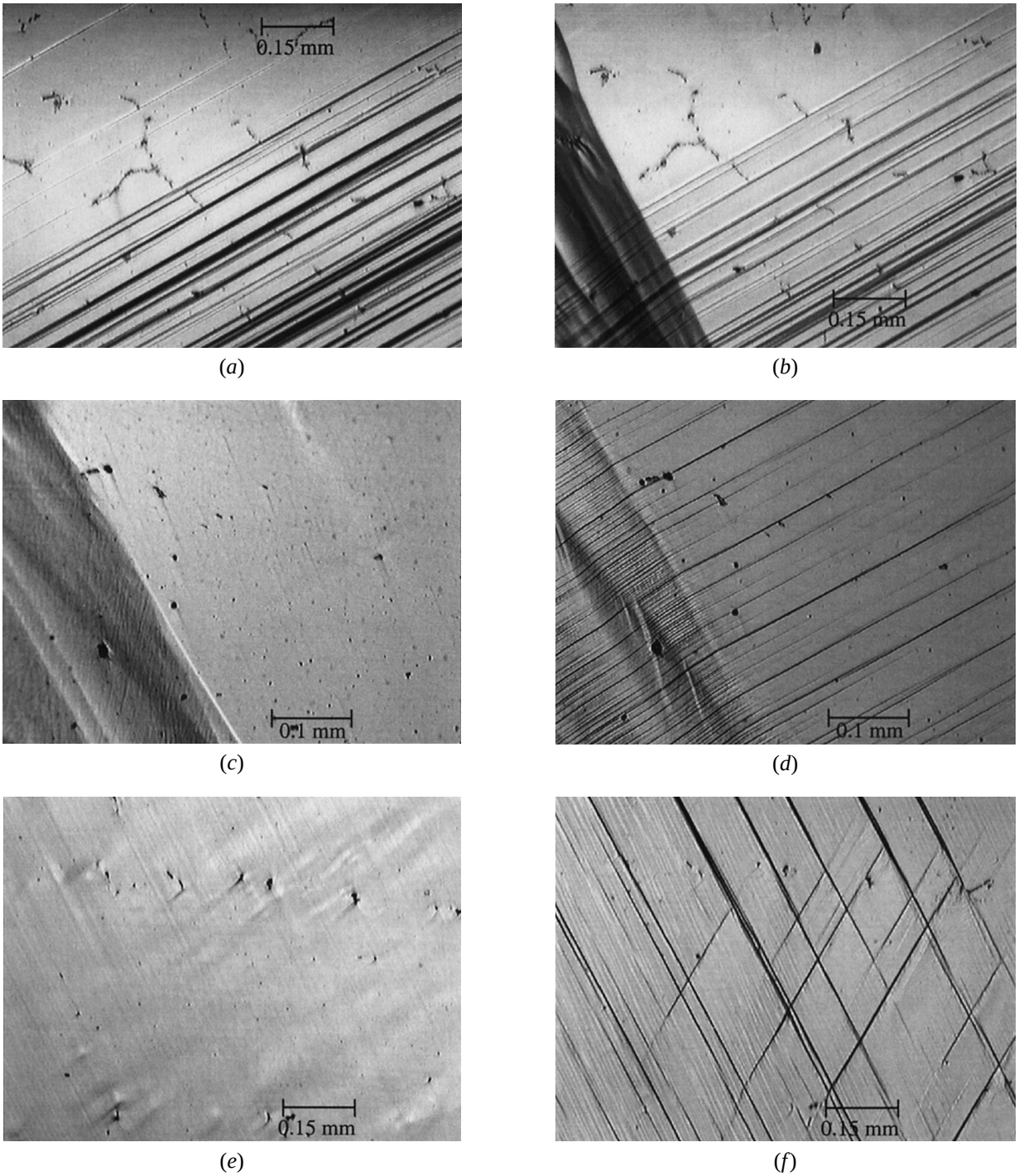

(*a*) (*b*) (*c*) (*d*) (*e*) (*f*)

Fig. 8—The surface relief patterns of the [$\bar{1}$23] orientation under (*a*) forward tension, (*b*) reverse compression, (*c*) forward compression, (*d*) reverse tension and of the [001] orientation under (*e*) forward tension, and (*f*) reverse compression. In (b) and (c), dark thick features are MSBs. The thin lines in (a), (b), (d), and (f) are twins. Two twin systems are evident in (f).

$$\sigma_{\text{rev}} = \sigma_0 + \sigma_d - \sigma_b \qquad [2]$$

Combining Eqs. [1] and [2] and then dividing σ_b by work-hardening results in our Bauschinger stress parameter (BP):

$$\text{BP} = \frac{\sigma_b}{\text{total work hardening}} = \frac{\sigma_f - \sigma_{\text{rev}}}{2(\sigma_f - \sigma_0)} \qquad [3]$$

This parameter is useful in comparing our results with dispersion-hardened fcc materials, such as Al-4 pct Cu.[3] In the limit such that $\sigma_b \to 0$, the BE vanishes, since there are no available long-range back stresses that would aid the reverse deformation. The other limiting case in which $\sigma_f \to \sigma_0$, such that the forest dislocation hardening (σ_d) and long-range back stress are not effective, is a somewhat ideal condition, since this initially requires a dislocation-free material and Lüder's type propagation of initial deformation.

Figure 9 demonstrates the BP *vs* forward strain responses of three orientations in both the FC/RT loading (Figure 9(a))

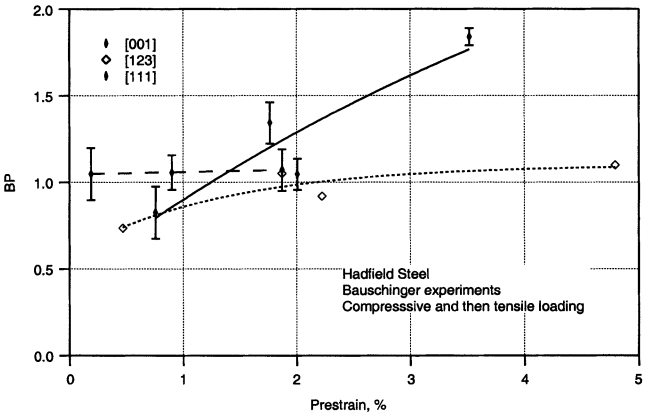

(*a*)

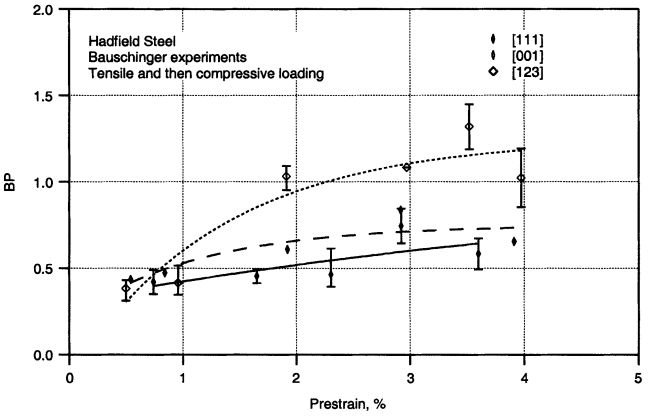

(*b*)

Fig. 9—The Bauschinger parameter based on remote stresses (BP) *vs* the strain in the forward loading (prestrain) plots of (*a*) FC/RT and (*b*) FT/RC loading schemes. For the definition of the parameter BP, refer to the main text (Eq. [3]). For some cases, error bars that are not indicated to keep the figures simple are presented in Fig. 11.

and FT/RC loading (Figure 9(b)) schemes. To determine the yield strengths for forward and reverse loadings, several strain offset values were used and 0.01 pct was chosen to construct Figure 9.

In Figure 9(a) the [001] orientation exhibits the highest BE under the FC/RT scheme. Since the specimen is deformed by twinning under compression, Figure 9(a) justifies our argument that twinning is a stronger barrier in developing long-range back stress than MSBs and dislocation tangles. The magnitude of the BE for this case increases with increasing prestrain. If further compressive strain (with no buckling) were possible in this case, the BE would saturate and start to decrease. In the case of the $[\bar{1}11]$ orientation with the FC/RT scheme, the compressive strains were held to 2 pct to avoid buckling. However, localization in the $[\bar{1}23]$ orientation under compression is not as severe as in the $[\bar{1}11]$ orientation, and thus it was possible to apply compressive strains as high as 5 pct for this case. The magnitude of the BE did not change with prestrain in the $[\bar{1}11]$ orientation with the FC/RT scheme at small strains, while it increased slightly and then saturated near 3 pct prestrain in the case of the $[\bar{1}23]$ orientation. The BE is higher in the $[\bar{1}11]$ case compared to the $[\bar{1}23]$ case because highly localized slip (MSB) in the $[\bar{1}11]$ orientation under compression forms

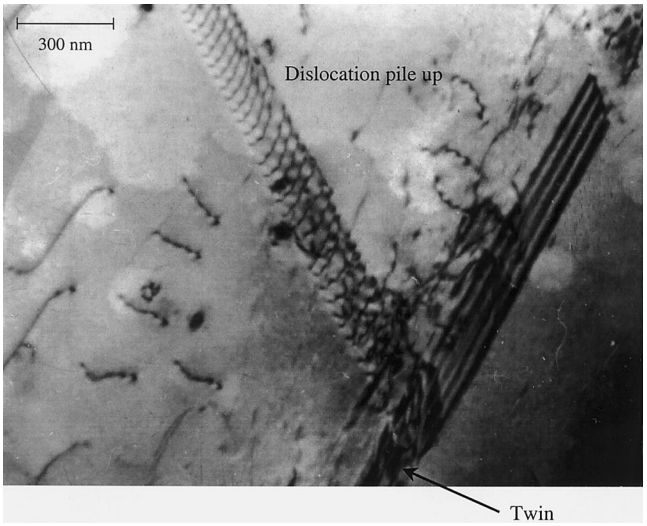

Fig. 10—Two-beam bright-field image showing the dislocation arrangement near a twin in the [111] orientation at 3 pct tensile strain. The region with the high dislocation density is the twin. Note the accumulation of dislocations near the twin boundary.

stronger dislocation walls with higher dislocation density and develops higher long-range back stresses.

The same trends were observed in Figure 9(b), which demonstrates the BP *vs* forward prestrain in the FT/RC scheme. The $[\bar{1}11]$ and $[\bar{1}23]$ orientations exhibit higher BE than the $[\bar{0}01]$ orientation, because in the forward loading, the former are deformed by macroscopic twinning (Figure 8(a)). The BE is higher in the $[\bar{1}23]$ case compared to the $[\bar{1}11]$ orientation. This is partly attributed to the differences in the volume fraction of twins formed (thus, the number of barriers to dislocation motion) and to the differences in the slip activities of the $[\bar{1}11]$ and $[\bar{1}23]$ orientations at the same strain level from microscopical investigations. Thus, the prestrain accomplished in the $[\bar{1}11]$ orientation is mostly due to twinning. However, in the $[\bar{1}23]$ case, slip plays an important role in the deformation. Higher dislocation density and pileups at the twin boundary trigger early yield in the reverse loading of the $[\bar{1}23]$ case. A representative TEM image of dislocation pile-up formation is presented in Figure 10 for the $[\bar{1}11]$ orientation at 3 pct tensile strain.

D. *Determination of BP Based on Resolved Shear Stresses*

Because single crystals were employed in the present study, it would be instructive to revise the BP representation using resolved shear stress components because of the orientation and stress-state dependence of deformation mechanisms. We note that, for high SFE fcc materials, such as Al and Cu, deforming only by slip, the BP would be the same regardless of whether applied or resolved components were used.

The BP was recalculated using resolved components (with Schmid factors from Table I), with the corresponding deformation modes as follows:

$$\mathrm{BP}_{\tau} = \frac{\tau_f - \tau_{\mathrm{rev}}}{2(\tau_f - \tau_0)} \qquad [4]$$

where the stresses represent the resolved components of

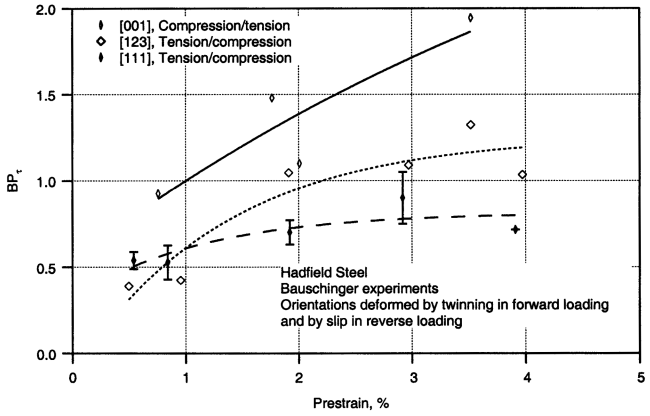

(*a*)

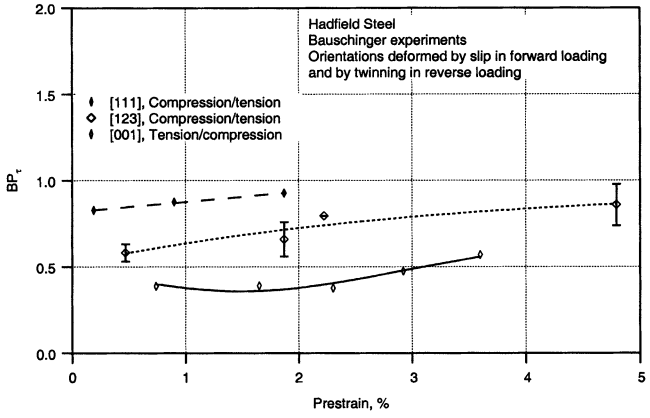

(*b*)

Fig. 11—The Bauschinger parameter based on resolved shear stresses (BP_τ) *vs* the strain in the forward loading (prestrain) plots of (*a*) twinning in forward and slip in reverse loading and (*b*) slip in forward and twinning in reverse loading schemes. For the definition of the BP_τ, refer to the main text (Eq. [4]). For some cases, error bars that are not indicated to keep the figures simple are presented in Fig. 9.

the ones in Eq. [3]. Figure 11(a) presents the orientations deforming by twinning in the forward loading, and slip in the reverse direction. The reverse cases, with slip in the forward and twinning in the reverse loading, are demonstrated in Figure 11(b)

E. *Discussion of the Bauschinger Experiments*

The aforementioned results clearly indicate the effects of twinning and the localized slip as well as the typical dislocation motion on the BE in a solid-solution-hardened, low SFE metal. The clear understanding of the interaction of these mechanisms is believed to improve the current understanding of work-hardening and cyclic deformation of low SFE steels that twin.

The large difference in the magnitude of the BP between Figures 11(a) and (b) is striking. The [001] orientation exhibited the highest difference in the BP levels of two different loading schemes, for two reasons. First, because this orientation deforms with homogeneous slip under tension (Figure 8(e)), the number of barriers that cause back stress accumulation are limited. Second, the activation of two twinning systems under compression creates strong barriers producing pile-up dislocations and, consequently, a larger back stress. This leads to both a high BE in the FC/RT scheme and a relatively low BE in the FT/RC scheme, providing the largest difference between the two loading schemes.

In Figure 11(b), it can be seen that MSBs (the $[\bar{1}11]$ and $[\bar{1}23]$ orientations with FC/RT) provide a larger BE than ordinary slip (the [001] orientation with FT/RC). The more slip is localized in the form of MSBs or dislocation walls, the higher is the BE.

The magnitude of the stress parameter in Figure 11(b) at small strains is larger than the one in Figure 11(a) for the orientations of $[\bar{1}11]$ and $[\bar{1}23]$. This is because the slip activity is not sufficient for building up a high back stress, while strain is achieved mostly by localized twinning, and twins are mostly coherent with the matrix. However, in the case of localized slip, MSBs serve as long-range back stress sources and assist reverse deformation. As strain increases, dislocations start to pile up at the twin boundaries, leading to incoherent twins; this results in a higher back stress.

The $[\bar{1}11]$ with tensile forward loading (Figure 11(a) demonstrates a lower BE than the one with compressive forward loading (Figure 11(b)). This supports our hypothesis that lack of slip activity does not generate enough back stress at the twin boundaries. The twin volume fraction in the former case is large, implying less slip activity, less dislocation pileup, and thus a low back stress and low BE.

Although the [001] orientation with the FT/RC scheme seems to demonstrate a small BE as compared to the other two orientations, the magnitude of the BP is much higher than the one observed in pure Cu single crystals (approximately 4 times higher).[7] It is as high as the one observed in the precipitation-hardened Al-4 pct Cu single crystals ($BP \cong 0.5$ for the [001] orientaion).[3] This is attributed to the fact that the chemical interaction between Mn and C atoms (formation of Mn-C couples) destroys the short-range order, decreases the friction stress,[17] and eases the reverse dislocation motion.

In summary, the present study proves that Hadfield steel single crystals can demonstrate as high a BE as dispersion-hardened alloys, because twinning and localized slip are strong barriers. Although these barriers, which can be penetrated at high stresses, are different from nondeformable hard inclusions, the pileups at the boundary and dislocation activity inside these regions produce sufficient long-range back stress to trigger lower yield strength. The stress concentration around these regions (twins and MSBs) and the orientation change accompanying these localized deformations also contribute to the BE. In light of these experimental findings, twinning will be considered as a permeable barrier to dislocation motion, and the forward and reverse stress-strain response of single crystals will be simulated by using a VPSC crystal plasticity model. This model is explained in our previous work, [12] and the essentials of the constitutive formulation will be explained in Section IV, as will the incorporation of twinning in the model.

IV. CONSTITUTIVE FORMULATION

The VPSC formulation together with a twinning reorientation scheme was first developed by Lebensohn and Tomé.[18] This formulation circumvents the restrictions of Taylor–Bishop–Hill and Relaxed Constraints formulations in incorporating twinning into the plasticity models. Moreover, the interaction of grains with each other and the interaction of

twinning and the matrix are of the utmost importance in any polycrystals model. The VPSC treats each grain or twin lamellae as a viscoplastic inclusion embedded in the homogeneous medium representing the aggregate.

We present the main formulation of the VPSC model here. More details can be found in Lebensohn and Tomé[18] and Karaman *et al.*[12] The constitutive law for the grain is based on a rate-sensitive criterion that expresses the shear rate in each deformation system as a power of the resolved shear stress in such a system. The total strain rate in a crystal can be written as the sum of all potentially active systems and can be pseudolinearized as follows:[18]

$$\dot{\varepsilon}_i = \left[\dot{\gamma}_0 \sum_1^s \frac{m_i^s \, m_i^s}{\tau_0^s} \left(\frac{m_k^s \, \sigma_k}{\tau_0^s} \right)^{n-1} \right] \sigma_j = M_{ij}^{c(\text{sec})}(\sigma)\sigma_j \qquad [5]$$

where $\dot{\gamma}_0$ is a reference rate; τ_0^s is the threshold stress corresponding to this reference rate, n is the inverse of the rate sensitivity index; m and σ are the vector representations of the Schmid and the remote stress tensors, respectively; s represents the slip or twinning systems; and k changes from 1 to 5. The $M_{ij}^{c(\text{sec})}$ is the secant viscoplastic compliance of the crystal, which gives the instantaneous relation between stress and strain rate.

At the macroscopic level, the polycrystal response is described with the same pseudolinear constitutive equation. If the $\dot{E}$ and Σ are the polycrystal strain rate and stress, respectively, the secant relation can be written as

$$\dot{E}_i = M_{ij}^{(\text{sec})}(\Sigma)\Sigma_j \qquad [6]$$

where $M^{(\text{sec})}$ is the secant compliance tensor for the polycrystal aggregate.

Defining the deviations in strain rate and stress between the inclusion and the overall magnitude as

$$\tilde{\dot{\varepsilon}}_k = \dot{\varepsilon}_k - \dot{E}_k \qquad [7]$$

$$\tilde{\sigma}_j = \sigma_j - \Sigma_j \qquad [8]$$

the solution of the viscoplastic inclusion problem leads to the interaction equation

$$\tilde{\dot{\varepsilon}} = -\tilde{M}{:}\tilde{\sigma} \qquad [9]$$

where the colon indicates tensor contraction and the interaction tensor $\tilde{M}$ is defined as

$$\tilde{M} = (I - S)^{-1}{:}S{:}M^{(\text{sec})} \qquad [10]$$

where S is the viscoplastic Eshelby tensor.

In this formulation, the viscoplastic modulus of the grain and of the homogeneous medium are assumed to be known in advance, which is not the case. Therefore, a self-consistent expression must be found from which the macroscopic modulus $M^{(\text{sec})}$ can be calculated by substituting Eqs. [5] and [6] in Eq. [9]. The macroscopic strain rate is evaluated by taking the weighted average of crystal strain rates over all the crystals as follows:

$$M^{(\text{sec})} = \langle M^{c(\text{sec})}{:}(M^{c(\text{sec})} + \tilde{M})^{-1}{:}(M^{(\text{sec})} + \tilde{M}) \rangle \qquad [11]$$

This equation gives the polycrystal compliance M and has to be added to the previous system in order to obtain an explicit solution of the problem. Equations [4], [8], and [10] are not solved simultaneously for all the grains, but an iterative procedure is used, which is described in Karaman *et al.*[12]

To predict a single crystal stress-strain response, a total of 1000 grains was used, and all grains initially had the same crystallographic orientation. This provides the scheme with statistical significance and allows for regions with the same orientation but different neighborhoods to favor different slip systems. As a result of this, boundary conditions were satisfied without imposing constraints, as in the case of Taylor–Bishop–Hill and Relaxed Constraints formulations.

The tracking of the reorientation of a grain by twinning, while keeping the previous deformation history of the grain, is performed by the Predominant Twin Reorientation (PTR) Scheme.[12,19] In this scheme, the real volume fraction of twinning f_R in the polycrystal aggregate is calculated considering the weighted average of twin activities in each grain. Whenever an entire crystal is reoriented by twinning, the effective twin volume fraction f_E is updated. At every deformation step, the accumulated twin volume fraction in the individual twinning systems of each grain is compared with a threshold value f_T. The characteristic of this scheme is that it favors the reorientation of crystals using the most active twinning systems. This is justifiable from the experimental findings, because at most two twin systems prevail in single crystals of Hadfield steel at small and moderate strains (Figure 8), and it is what simulations predict with the current reorientation scheme. The rest of the twinning activity is considered as pseudoslip to satisfy compatibility conditions.

In Section V, modeling approaches will be discussed related to the present study of the BE.

V. STRAIN-HARDENING FORMULATION

In the crystal plasticity models, the consideration of a physical length scale in relation to microstructural parameters (such as dislocation mean free path) is mostly lacking. In recent years, models have been proposed[20,21,22] to address this issue. However, the incorporation of twinning and the interaction of twinning and slip are still unresolved. The authors' recent treatment[12] of the role of twinning in the strain hardening in the same material as used in the present study has considered the twin boundaries as barriers to dislocation motion. The model subdivides the grains during deformation and the mean free path decreases with increasing volume fraction of twins.

What follows are the main equations of this approach. We consider an evolution equation for the dislocation density following Estrin and Mecking[21] and Acharya and Beaudoin[22] in the form

$$\dot{\rho} = \sum_k \left\{ \frac{K_0}{d\,\mathrm{b}} + k_1\sqrt{\rho} - k_2\rho \right\} |\dot{\gamma}^k| \qquad [12]$$

where d is the distance between twins, b is the Burgers vector, k_1 and k_2 are constants, and K_0 is a geometric constant. The first term represents an empirical geometric storage term due to twin boundaries, and the second term represents the athermal (statistical) storage of moving dislocations. The dynamic recovery is represented with the third term. Twins are very narrow in the present material and the spacing between twins is almost constant,[10] and thus, the mean free path is constant as well.

The flow stress at a finite temperature and strain rate is

defined following Kocks *et al.*,[23] Kocks,[24] and Mecking and Kocks,[20] along with the Bailey–Hirsch relationship as

$$\hat{\tau} - \hat{\tau}_0 = \alpha\mu b \sqrt{\rho} + \hat{\tau}_i \qquad [13]$$

where $\hat{\tau}_0$ is the initial yield strength, which considers initial dislocation density, temperature, and strain rate; α is a constant; μ is the shear modulus; and $\hat{\tau}_i$ is the contribution of solid solution hardening. Because the nature of the interaction of the terms has not been completely understood to date, a simple superposition is used following Kocks *et al.*[23]

Upon combining Eqs. [12] and [13], and with the distance d between neighboring twins evaluated from Fullman's volumetric analysis,[25]

$$\frac{1}{d} = \frac{1}{2t}\frac{f}{1-f} \qquad [14]$$

where t is the thickness of twins; and, differentiating with respect to time, we obtain the following expression for single crystal hardening:

$$\dot{\hat{\tau}} = \left[\frac{K_0\alpha^2\mu^2 b}{4(\hat{\tau} - \hat{\tau}_0)}\frac{1}{t}\frac{f}{1-f} + \left\{\frac{\alpha\mu b}{2}k_1 - k_2\frac{\hat{\tau} - \hat{\tau}_0}{2}\right\}\right]\sum_k |\dot{\gamma}^k| + \dot{\hat{\tau}}_i \qquad [15]$$

The last term is the well-known Voce-form hardening, which can be written as[26]

$$\dot{\hat{\tau}} = \left[\frac{K_0\alpha^2\mu^2 b}{4(\hat{\tau} - \hat{\tau}_0)}\frac{1}{t}\frac{f}{1-f} + \theta_0\left\{\frac{\hat{\tau}_s - \hat{\tau}}{\hat{\tau}_s - \hat{\tau}_0}\right\} + \frac{\partial\hat{\tau}_i}{\partial\gamma}\right\}\sum_k |\dot{\gamma}^k| \qquad [16]$$

where θ_0 is the constant strain-hardening rate and $\hat{\tau}_s$ is the saturation stress in the absence of geometric effects.

In the present material, dynamic recovery is not a significant softening mechanism at room temperature.[12] Therefore, the Voce term in Eq. [16] is not critical in the present case and is ignored. The solid-solution-hardening contribution $\hat{\tau}_i$ to the flow stress should include the magnitude of solid solution content, the type of solution (interstitial or substitutional), and the misfit parameters (size or modulus). However, in the presence of the slip-twin interaction, solid solution hardening plays a secondary role in hardening. Therefore, the last term in Eq. [16] is only significant for stage I of the stress-strain behavior of the single crystals, and it is taken constant as a first approximation following Seeger.[27]

A. *Microstrain Regime*

When the forward stress–true strain responses. (Figures 1 through 6) of all orientations are investigated closely, two distinct regimes are evident. The first region at small strains demonstrates a high strain-hardening behavior, while the second one follows a typical fcc single crystal response corresponding to a Lüder's type propagation of local deformation. As shown in an earlier study,[15] the single crystals of the current material demonstrate both large micro- and macrodeformation regimes during straining. It is shown that the extent of this region is orientation dependent.

The reasons for this microyielding and high strain hardening are twofold. The extended stacking faults, together with statistical microtwin formations, are responsible for the microyielding. The high constraint provided by the surrounding interstitially hardened elastic medium hinders the growth of the microtwins and the macroscopic glide of partial or perfect dislocations.[15] The high interstitial carbon content (5 at. pct) imparts high friction stress to the Hadfield steel. This theory is valid for the orientations and stress states in which the applied stress-state increases the partial dislocation separation (Copley–Kear effect).[28] The effect of applied stress on the separation of partials, and thus the extent of stacking fault, helps the nucleation of macroscopic twins. As an example, Table I of Karaman *et al.*[15] demonstrates that, for the orientations $[\bar{1}11]$ and $[\bar{1}23]$ under tension, the difference between macroscopic and microscopic yield strengths is around 70 MPa; it is 40 MPa in the [001] orientation under tension. The applied stress helps to extend partial dislocation separation distance in the first two, while it has a reverse effect on the third. Therefore, it is possible to deduce that, in the orientations deforming by twinning, an extended microstrain region will likely be observed.

The aforementioned increase in partial separation distance by an applied stress is significant if applied stress levels are high for materials with low and medium SFE. If the material has a very low SFE, as do Cu-Al alloys, even small stress levels can have a significant effect on the separation distance. Abel and Muir[9] argued that the effect of the applied stress on the partial separation distance is the main reason for the observed large BE on their low-SFE Cu-Al alloys (SFE $<$ 10 mJ/mm^2).

A possible second explanation of the microstrain region could be linked to the difference between the elastic interactions of screw and edge dislocations in the presence of high solid solution content.[29] Elastic interaction of a solute atom or atom clusters with edge dislocation is considerably stronger than a screw dislocation. This results in the edge component of a dislocation being pinned, while the screw component is free to glide.[29,30] Long *et al.*[30] used a similar idea to explain microyielding of Cu-0.4 pct Cr single crystals. Between micro- and macroyield points, screw components of dislocation loops glide, while edge components are hindered by the Cr particles. In the present material, carbon atoms provide a similar hindrance, and, at small strains, dislocations have edge character, as can be seen in Figure 12. In this figure, dislocations are long, which implies that before edge components are freed, screw components glide significantly, providing an extended micro-macroyield transition.

No matter which mechanism has a more significant effect in this transition region, it is possible to define strain hardening with a dynamic saturation behavior similar to the well known dynamic recovery formulation of fcc materials, as forwarded by Mecking and Kocks.[20] The strain hardening in the microstrain region was described with the following empirical relation:

$$\theta^{\text{micro}} = \theta_0^{\text{micro}}\left\{\frac{(\hat{\tau}_s)_{\text{micro}} - (\hat{\tau})_{\text{micro}}}{(\hat{\tau}_s)_{\text{micro}} - (\hat{\tau}_0)_{\text{micro}}}\right\} \qquad [17]$$

where $(\hat{\tau}_0)_{\text{micro}}$ is the microyield strength, $(\theta_0)_{\text{micro}}$ is the constant strain-hardening rate, and $(\hat{\tau}_s)_{\text{micro}}$ is the saturation stress, which is the macroyield strength in the present case.

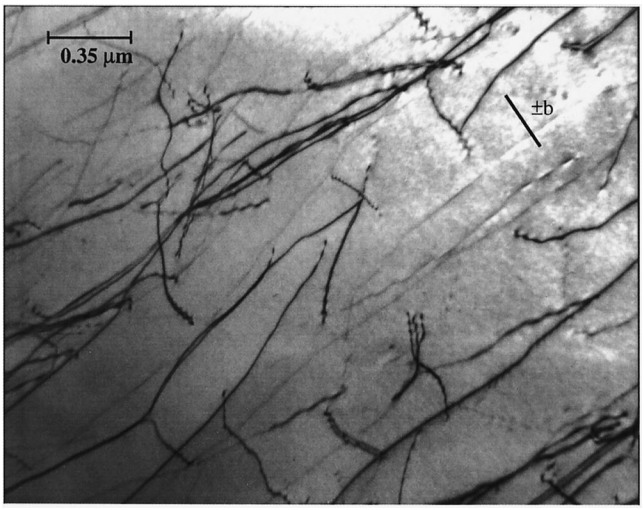

Fig. 12—Two-beam TEM bright-field image showing dislocation arrangement in the sample deformed in tension along the [$\bar{1}$23] orientation at 3 pct strain. For long straight dislocations, most of which have almost pure edge characters, the prevailing Burgers vector is indicated. The absence of pileups is worthy of note.

The proposed microhardening law was used to track the stress in each deformation step in the simulations, together with other hardening mechanisms. In the simulation of the reverse loading of Bauschinger experiments, the microstrain-hardening law is relaxed for dislocation pileups in forward loading, because they are assumed to have edge character and are not suitable for the microyielding.

Adding the microstrain-hardening expression in Eq. [17] to Eq. [16], the final version of the stress evolution is expressed as

$$\dot{\hat{\tau}} = \left[(\theta_0)_{\text{micro}} \left\{ \frac{(\hat{\tau}_s)_{\text{micro}} - \hat{\tau}}{(\hat{\tau}_s)_{\text{micro}} - (\hat{\tau}_0)_{\text{micro}}} \right\} + \frac{K_0 \alpha^2 \mu^2 \mathbf{b}}{4(\hat{\tau} - \hat{\tau}_0)} \frac{1}{t} \frac{f}{1-f} + \theta_0 \left\{ \frac{\hat{\tau}_s - \hat{\tau}}{\hat{\tau}_s - \hat{\tau}_0} \right\} + \frac{\partial \hat{\tau}_i}{\partial \gamma} \right] \sum_k |\dot{\gamma}^k| \quad [18]$$

B. *The Calculation of Back Stress*

In the present study, the approaches of Brown and Clarke,[14] Moan and Embury,[3] and Pedersen *et al.*[7] were modified to calculate the back stress accumulated in forward straining.

Twinning produces incompatibility in plastic deformation at the local level arising from the boundary misorientation and incoherency of the twin and the matrix. Incoherency is accommodated by dislocations at twin-matrix boundaries leading sessile dislocations at the boundaries, as demonstrated microscopically by Remy.[25] It is well known that twin boundaries are a particular case of grain boundaries with a low coincidence index, $\Sigma = 3$, and are suitable for dislocation accumulation, as seen in Figure 10.

In the light of the preceding facts, at small strains, the dislocations that are noncoplanar to the existing twins are assumed to nucleate and to accumulate near twin boundaries. The slip activity and dislocation density of noncoplanar dislocations are orientation dependent and thus, in the number of dislocations piled up at the boundary is orientation dependent as well. Dislocations coplanar to twinning do not form pileups and do not generate the long-range back stress. Therefore, it is possible to use the model of Brown and Clarke,[14] which assumes that twins are inhomogeneities in the matrix. In the Brown and Clarke model, the back stress on the active slip systems is calculated as

$$\tau_{\text{back}} = 2\chi f \mu \varepsilon_p^* D \quad [19]$$

where χ is the Eshelby accommodation factor; f is the volume fraction of twins nucleated during forward loading and thus dependent on the magnitude of prestrain; and ε_p^* is the unrelaxed shear strain in a particular slip system built up during forward loading and is proportional to the slip activity in the forward loading. Because strain levels are small in the present study, accumulated dislocations are not likely to be relaxed. The modulus correction term due to twinning is D: it is also orientation dependent because of the orientation dependency of the single crystal moduli. Twins are assumed to have a disc shape. The factor χ is taken to be 1/2, from Table IV of Brown and Clarke,[14] considering the component of the Burgers vector of a slip system perpendicular to twins. Because dislocations perpendicular to the twinning system form pileups, the unrelaxed shear strain ε_p^* can be expressed as

$$\varepsilon_p^* = \varepsilon_p \sin \beta \quad [20]$$

where β is the angle between the slip systems and twin planes.

The present formulation assumes that the obstacle (twinning) density or structure is unchanged by the initial reverse flow and remains stable (no elastic twinning). Equation [19] successfully follows the general trend of back stress in the orientations and stress states with a large BE, as shown in Figures 9 and 11. The BP saturates at high prestrain values (Figure 11), and in Eq. [19] the terms f and ε_p^* compensate each other at higher strains to mimic this saturation, *i.e.*, when f is large, then slip activity ε_p^* is low, or *vice versa*. The predicted back stress in the VPSC simulations was as high as 75 MPa in the case of [001] compression at a strain level of 3.5 pct.

VI. THE COMPARISON OF SIMULATIONS AND EXPERIMENTAL RESULTS

To evaluate back stress evolution, microstrain hardening, and hardening due to twin-slip interaction approaches, three orientations have been chosen under forward loading conditions. Twinning is the primary deformation mechanism at the onset of deformation in these three cases. These include the [$\bar{1}$11] and [$\bar{1}$23] orientations under tensile forward loading and the [001] orientation under compressive forward loading.

Initial micro- and macrocritical resolved shear stresses (CRSS) for both slip and twinning were obtained from the experimental results. The microsaturation stress is taken to be equal to the macroyield stress such that, whenever the edge dislocations can no longer be pinned by obstacles and start total dislocation gliding, or whenever the expansion of the partial dislocations saturates and partials glide together, macroyielding starts. The rate sensitivity n is chosen to be 20, as in Eq. [5].

Because twinning starts at strains as low as 1 pct in

forward loading, the twinning reorientation scheme is activated early to be consistent with the experimental observations. Because the initial macrohardening rate is small due to a Lüder's type propagation, $\partial\hat{\tau}_i/\partial\gamma$ of Eq. [18] is taken as $\mu/4000$ for both slip and twinning. The initial value of the micro CRSS is set to $(\hat{\tau}_0)_{\text{micro}} = 110$ MPa for slip. The macro CRSS, $\hat{\tau}_0$, and thus the microsaturation stress $\hat{\tau}_s$ for slip, was chosen to be 160 MPa. The CRSS is 155 MPa for twinning. The microstrain-hardening coefficient is taken as $(\theta_0)_{\text{micro}} = \mu/10$. Twins are very narrow and remain at a constant width of 100 to 200 nm during deformation.[10,12] Therefore, the thickness t in the hardening term in Eq. [18] originating from the dislocation storage is set to 100 nm; the value of α is 1/3.[31] The term K_0 is 0.1 for the present orientations.

In the reverse loading simulations, the values are maintained constant and the back stress term in Eq. [19] was introduced to reduce the CRSS on the activated slip systems, which were noncoplanar to nucleated twin planes in the forward loading. The same back stress was used for twin systems planar to slip planes activated in the forward loading. However, since Schmid factors of twinning are considerably lower for the present orientations under reverse loading, no twin activity is predicted. The stored twinning volume fraction and the shear strain in each active system in forward loading were used for the calculation of the back stress in reverse loading for each of three cases.

The corresponding simulations for the aforementioned cases are presented in Figures 1 through 3. In Figure 1, the stress-strain response of the $[\bar{1}11]$ orientation with FT/RC scheme forward loading was used to determine the preceding constants. In reverse loading, the simulations are conducted with and without back stress. As noted in Figure 1, the back stress has a significant effect on reverse yielding.

There is good agreement between the experimental results and prediction for these three cases. The strain-hardening differences between them on both forward and reverse loading originate from the number of systems activated. In the $[\bar{1}23]$ orientation with FT/RC scheme, strain hardening is considerably lower than for the other two orientations because only a single system is active for both slip and twinning. However, in the other two cases, although one twinning system is primarily active (in experiments and predictions), multiple slip systems are active along with a small secondary twinning formation.

Moreover, the back stress has a mainly transient effect on the reverse yielding, except for the $[\bar{1}11]$ case. In the $[\bar{1}23]$ orientation, the back stress leads to a transient effect that does not affect macroscopic yield strength. This can be seen better when Figures 3 and 5 are compared. Although the back stress has a similar effect in the $[\bar{0}01]$ orientation as well, the macroyield strength appears the same when Figures 2 and 6 are compared. Strain-hardening characteristics are different between forward tensile (Figure 6) and reverse tensile (Figure 2) loading cases. In the reverse tensile loading, strain hardening is significantly lower, indicating either that fewer slip systems are active or that the resistance to flow is lower than the forward tensile loading case. This implies that only a certain number of slip systems form pileups at the twin boundaries, and during reverse loading, these systems are easier to activate because of the reduction of their critical stresses. Because of the latent and forest hardening, other possible systems having the same Schmid factors cannot be activated.

On the other hand, the back stress leads to both a transient and permanent softening in the $[\bar{1}11]$ orientation with FT/RC scheme. This is because there exist more twin boundaries at which to store dislocations to trigger the reverse yielding, and the density of the sites in which slip starts is larger than in the $[\bar{1}23]$ case. It can easily be seen with optical microscopy observations that the density of twins is higher in the $[\bar{1}11]$ orientation. Moreover, MSB formation is more pronounced in the $[\bar{1}11]$ case of reverse compressive loading because of the number of slip systems activated.

VII. CONCLUSIONS

In the present study, the three orientations ($[\bar{1}11]$, $[\bar{1}23]$, and [001]) of Hadfield steel have been investigated and the role of stress direction, orientation, deformation mechanisms, and the prestrain level on the Bauschinger effect has been revealed by monotonic loadings and simulations. The work supports the following conclusions:

1. Whenever twinning is the primary deformation mechanism in forward loading (the $[\bar{1}11]$ and $[\bar{1}23]$ orientations under tension and the [001] orientation under compression), there is a significant lowering in the reverse yield strength, and thus a large Bauschinger effect. If twinning is followed by localized slip (MSB formation during the reverse loading of the $[\bar{1}11]$ orientation under FT/RC loading scheme), permanent softening (as defined in Figure 1) is observed. The homogeneous slip in the reverse loading following twinning results in a lower BE (the [001] orientation under FC/RT loading).
2. If localized is the deformation mechanism in the forward loading (the $[\bar{1}11]$ and $[\bar{1}23]$ orientations under compression), it generates a transient effect in the reverse stress-strain response by assisting the early dislocation motion. If the slip localization is not the case, no significant BE is observed, as in the case of [001] orientation under FT/RC loadings compared to other orientations.
3. The high BE in the present material is attributed to the long-range back stress originated by dislocation pileups accumulated at twin and MSB boundaries. These boundaries are considered as hard but deformable obstacles.
4. The Hadfield steel single crystals exhibit a higher BE than pure fcc alloy single crystals, such as Cu and Al, and the precipitation-hardened Al-4 pct Cu single crystals. Twinning is concluded to be a strong barrier to dislocation motion at low strains, which leads to accumulation of back stress at the boundary, similar to grain boundaries.
5. The unique strain-hardening approach and the back stress calculations introduced in the VPSC formulation have been proved to be useful tools for the prediction of the stress-strain behavior and the BE in interstitial solid-solution-hardened, low SFE steels. The predicted back stress was as high as 75 MPA in the [001] orientation under compression. The model correctly predicts the effect of the volume fraction of twins and the number of active slip systems on the BE and strain hardening.

ACKNOWLEDGMENT

This work was supported by the National Science Foundation Contract No. CMS 99-00090, Mechanics of Materials

Program (Arlington, VA). Professor Chumlyakov's work received support from The Russian Ministry of Education (1998–2000, MATI, Moscow). The facilities at Microanalysis of Materials, Materials Research Laboratory, The University of Illinois, were used. This laboratory is funded by DOE-DMS Grant No. DEFG02-96ER45439.

REFERENCES

1. J. Bauschinger: *Mitt. Mech. Tech. Lab. München*, 1886, vol. 13, pp. 1-115.
2. P.S. Bate and D.V. Wilson: *Acta Metall.*, 1986, vol. 34, pp. 1097-1105.
3. G.D. Moan and J.D. Embury: *Acta Metall.*, 1979, vol. 27, pp. 903-14.
4. S.N. Buckley and K.M. Entwistle: *Acta Metall.*, 1956, vol. 4, pp. 352-61.
5. A. Abel and R.K. Ham: *Acta Metall.*, 1966, vol. 14, pp. 1489-94.
6. J.D. Atkinson, L.M. Brown, and W.M. Stobbs: *Phil. Mag.*, 1974, vol. 30, pp. 1247-80.
7. O.B. Pedersen, L.M. Brown, and W.M. Stobbs: *Acta Metall.*, 1981, vol. 29, pp. 1843-50.
8. D.V. Wilson and P.S. Bate: *Mater. Forum*, 1987, vol. 10, pp. 33-42.
9. A. Abel and H. Muir: *Phil. Mag.*, 1973, vol. 27, pp. 585-94.
10. I. Karaman, H. Sehitoglu, K. Gall, Y.I. Chumlyakov, and H.J. Maier: *Acta Mater.*, 2000, vol. 48, pp. 1345-60.
11. A. Abel: *Mater. Forum*, 1987, vol. 10, pp. 11-26.
12. I. Karaman, H. Sehitoglu, A.J. Beaudoin, Y.I. Chumlyakov, C.N. Tomé, and H.J. Maier: *Acta Mater.*, 2000, vol. 48, pp. 2031-47.
13. G. Masing: *Wiss. Veröff. Siemens-Konzern*, 1923, vol. 3, pp. 231-39.
14. L.M. Brown and D.R. Clarke: *Acta Metall.*, 1975, vol. 23, pp. 821-30.
15. I. Karaman, H. Sehitoglu, K. Gall, and Y.I. Chumlyakov: *Scripta Mater.*, 1998, vol. 38, pp. 1009-15.
16. E.I. Litvinova, Y.I. Chumlyakov, H. Sehitoglu, and I. Karaman: *Physical Mesomech.*, 1999, vol. 2 (1–2), pp. 107-12.
17. W.S. Owen and M. Grujicic: *Acta Mater.*, 1999, vol. 47, pp. 111-26.
18. R.A. Lebensohn and C.N. Tomé: *Mater. Sci. Eng. A*, 1993, vol. 175, p. 71.
19. C.N. Tomé, R.A. Lebensohn, and U.F. Kocks: *Acta Metall. Mater.*, 1991, vol. 39, p. 2667.
20. H. Mecking and U.F. Kocks: *Acta Metall.*, 1981, vol. 29, p. 1865.
21. Y. Estrin and H. Mecking: *Acta Metall.*, 1984, vol. 32, p. 57.
22. A. Acharya and A.J. Beaudoin: *J. Mech. Phys. Solids*, *48*, 2000, vol. 10, pp. 2213-30.
23. U.F. Kocks, A.S. Argon, and M.F. Ashby: *Progr. Mater. Sci.*, 1975, vol. 19, pp. 1-291.
24. U.F. Kocks: in *Strength of Metals and Alloys*, P. Haasen, V. Gerold, and G. Kostorz, eds., Pergamon Press, Oxford, United Kingdom, 1979, p. 1661.
25. L. Remy: *Acta Metall.*, 1978, vol. 26, p. 443.
26. U.F. Kocks, C.N. Tomé, and R.H. Wenk: *Texture and Anisotropy*, Cambridge University Press, Cambridge, United Kingdom, 1998.
27. A. Seeger: *Structure and Mechanical Properties of Metals*, HMSO, London, 1963, p. 4.
28. S.M. Copley and B.H. Kear: *Acta Metall.*, 1968, vol. 16, p. 227.
29. R.L. Fleischer and W.R. Hibbard: *Structure and Mechanical Properties of Metals*, HMSO, London, 1963, p. 262.
30. N.J. Long, M.H. Loretto, and C.H. Lloyd: *Acta Metall.*, 1980, vol. 28, p. 709.
31. F.R.N. Nabarro, Z.S. Basinski, and D.B. Holt: *Adv. Phys.*, 1964, vol. 13, p. 193.